

ISSN: (Print) (Online) Journal homepage: <https://www.tandfonline.com/loi/tcie20>

## Automatic system design for flange surface quality inspection with a bionic motion-vision paradigm

Xiaoye Shen , Liang Gong , Xudong Li , Zhengwei Qin , Yuan Wei , Chengliang Liu & Jiaqi Zhang

To cite this article: Xiaoye Shen , Liang Gong , Xudong Li , Zhengwei Qin , Yuan Wei , Chengliang Liu & Jiaqi Zhang (2020): Automatic system design for flange surface quality inspection with a bionic motion-vision paradigm, *Journal of the Chinese Institute of Engineers*, DOI: [10.1080/02533839.2020.1819430](https://doi.org/10.1080/02533839.2020.1819430)

To link to this article: <https://doi.org/10.1080/02533839.2020.1819430>



Published online: 21 Sep 2020.



Submit your article to this journal 



View related articles 



CrossMark

View Crossmark data 



# Automatic system design for flange surface quality inspection with a bionic motion-vision paradigm

Xiaoye Shen<sup>a</sup>, Liang Gong<sup>a</sup>, Xudong Li<sup>a</sup>, Zhengwei Qin<sup>a</sup>, Yuan Wei<sup>a</sup>, Chengliang Liu<sup>a</sup> and Jiaqi Zhang<sup>a,b</sup>

<sup>a</sup>School of Mechanical Engineering, Shanghai Jiao Tong University, Shanghai, China; <sup>b</sup>Suzhou HULK Robot Co. Ltd, Suzhou, China

## ABSTRACT

Flanges are used to make connections. Their surface quality determines the joint mechanical strength and characteristics, while their defects lead to device failure. Complex surfaces and surface flaws pose challenges to automatic optical inspection (AOI) and conventionally, visual and manual inspection is employed. The aim of this study is to develop an automatic defect detection system for the flange surface, an operational pipeline with a bionic motion-vision mechatronic system, which mimics manual detection. Three methods are proposed as part of the system. The visual-detection-simulating sensing method, mimicking humans defect detection under horizontal light, is proposed to produce images of the defects on multifaceted reflective-metal surfaces. The human-operation simulation method, mimicking human defects detection under different light angles, is designed to optimize the visual perspective angles. The intelligent decision mechanism, mimicking the way human attention is focused, is proposed to solve complex pattern recognition problems. Based on this approach, an automated inspection machine, including posture adjustment, lighting, and imaging, for flange surface quality is developed. An intelligent inspection system with defect recognition algorithms is deployed. The smallest width of surface defects detected is 0.1 mm. The proposed apparatus design paradigm provides a general solution for flaw-detection on non-planar, complex surface workpieces.

## ARTICLE HISTORY

Received 22 February 2020  
Accepted 31 August 2020

## KEYWORDS

Automatic optical inspection (AOI); surface defects; bionic design; complex surface workpieces

## 1. Introduction

A flange is a common sealing connector, prone to surface defects that lead to connection and leakage failures (Kong et al. 2017). Because of its critical role in connection, quality inspection of the flange is essential. It is usually carried out manually, however, work fatigue can lead to unsatisfactory fault detection. Moreover, the inspection of a large number of flanges each day is expensive and labor-intensive. Currently, there are no suitable automated methods to replace manual work. An automatic apparatus for flange surface quality inspection is urgently required.

Conventional methods detect defects according to the physical properties of the material. The magnetic field method detects scratch pits (Gusev 2015), plastic deformations of the steel plates (Grijalba and Padovese 2018), and cracks in the welds (Kasai and Miura 2012). The radiant light method detects defects according to temperature changes (Sugimoto and Kawaguchi 1998). The ultrasonic method is generally used to measure the inside of a pipe (Da et al. 2018; Guo et al. 2015). It also performs well in long-range defect diagnosis of metallic structures (Abbas and Shafee 2018). In addition to the classic methods, 3D imaging techniques such as the grating method (Ye et al. 2018) and point cloud method (Jovančević et al. 2017) reconstruct a 3D model of the target, which is suitable for reflective metal surfaces (Xu, Gao, and Jiang 2018). Automatic optical inspection (AOI) methods are widely used for surface defect detection through image acquisition and analysis, such as mobile phone surfaces (Zhou et al. 2019), tile surfaces

(Hanzeai, Afshar, and Barazandeh 2017), cylinders (Chiou and Li 2009), metal ball surfaces (Lu, Zhao, and Qu 2006), reflective surfaces (Öztürk and Akdemir 2018), light guide plates (Huang and Chiu 2009) and other complex surfaces (Wang, Wen, and Song 2017).

Factors making defect detection a challenge are identified from the manufacturers' flange failure catalog. A flange possesses a complex structure with holes, rings, shoulders, steps, chamfers, and other 3D structures. 3D imaging technologies will face significant challenges in modeling flanges. Furthermore, a metal flange has reflections and shadows on the surface. At the same time, due to uses and processing technologies, surface roughness and texture are inconsistent. For example, the step on the upper surface to be welded to a pipe is smooth, whereas the lower surface for sealing is rough. Under these disturbances, both traditional and template-matching methods encounter problems in which defects and noise are indistinguishable at the same order of magnitude. AOI requires an optimized light source, for example, a polarized-light filter to enhance the contrast of defective images (Xu et al. 2017). Therefore, the detection method should be based on the extraction of the image features and edges of defects. In addition, the locations and shapes of defects are uncertain. There are more than a dozen types of defects in the catalog (Figure 1), which are difficult to identify. In this research, our focus is on the detection of frequent defects, such as scratch, imprint and burr.

In summary, the inspection apparatus requires an optimized lighting system to eliminate the negative impact of metal



**Figure 1.** Typical defects of flanges.

characteristics, an imaging platform to acquire clear images of the full viewing angle of flanges dynamically, and robust algorithms to identify the defects.

Inspired by the manual detection philosophy, the bionic motion-vision system design paradigm is proposed. Based on machine vision, it simulates the behavior of skilled industrial workers from the aspects of perspective selection, observation, and recognition, which realizes the detection of small flaws on the surface of complex structural flanges. The method can be divided into three major bionic parts: visual-detection-simulating sensing, human-operation simulating and human-visual decision mechanisms.

The AOI system with the bionic methods is described in Section 2. The experimental platform built to realize automatic surface defect detection is introduced in Section 3. The test results are presented in Section 4. Finally, Section 5 presents the conclusions of the study.

## 2. Method

To inspect the defects on reflective and multifaceted flanges with optimal view angles, an AOI system combining the advantages of manual detection and machine vision is designed. The detection methods can be divided into three major bionic parts: (a) Visual detection-simulating sensing method: The system would mimic workers who detect defects under horizontal light. A set of light sources capable of minimizing reflections and noise is designed to improve image quality. (b) Human-operation simulating method: The system would mimic workers who detect defects under different light angles. The rotating platform and air pump flipping system realize a multi-view scanning method. (c) Human-visual decision mechanism: The system would mimic the way human attention is focused. The segmentation algorithm replicates the human experience of defect detection. Figure 2 provides a structure diagram of the AOI system, which illustrates the three bionic methods and three working stations.

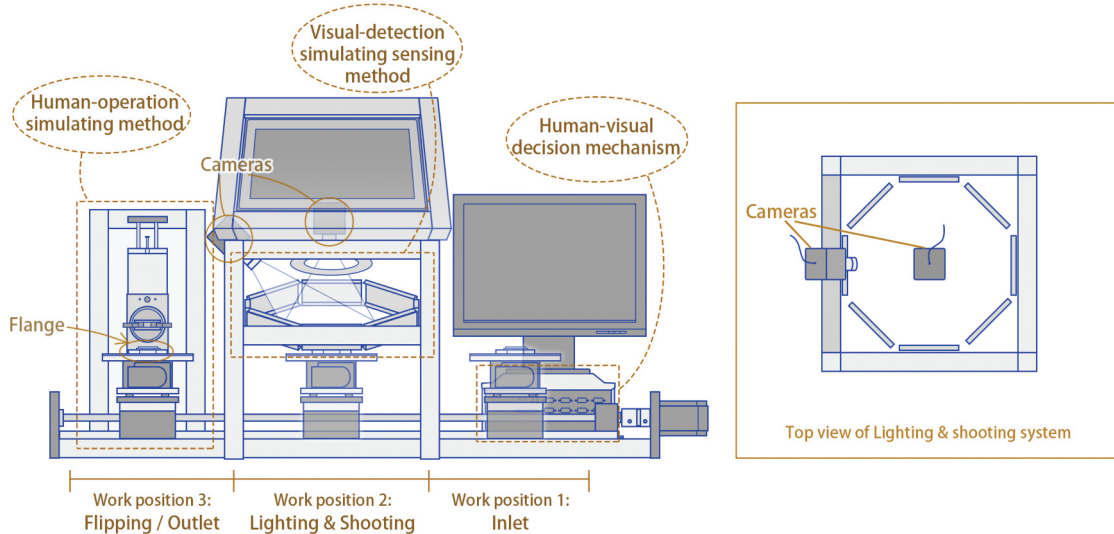


**Figure 2.** Structure diagram of AOI system.

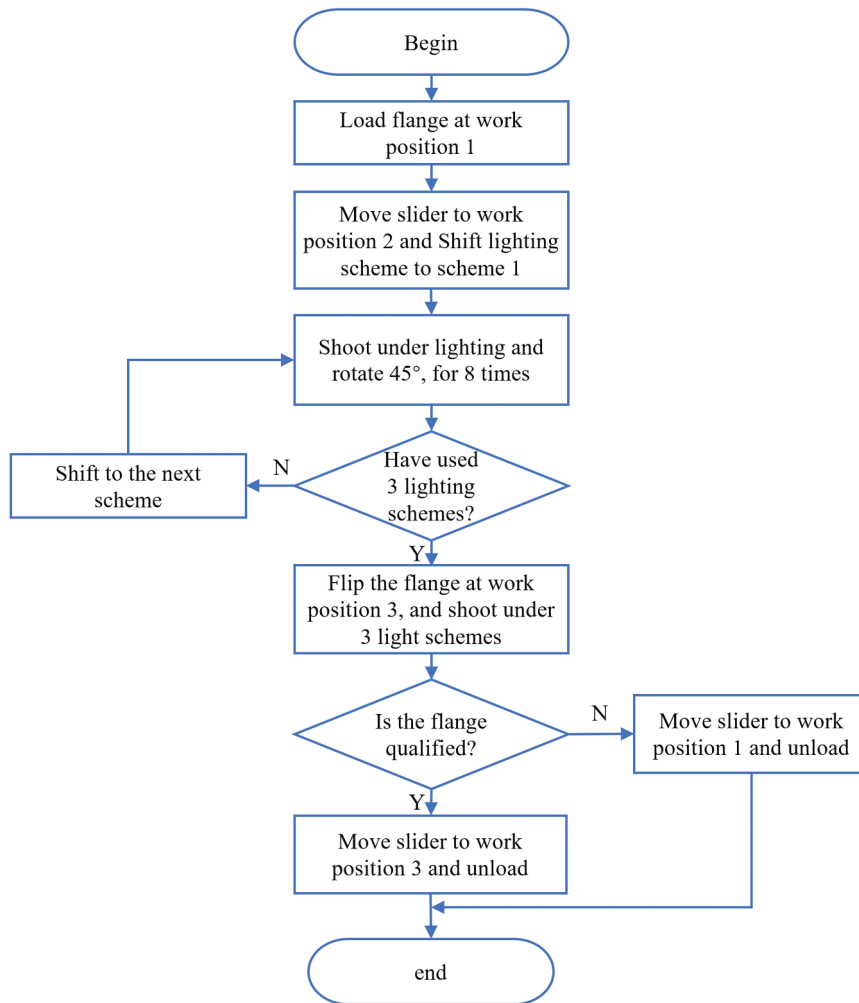


**Figure 3.** Work flow of the detection process.

Figure 3 illustrates the workflow of the detection process. A flange is transported from the inlet to the lighting platform. After taking full view images of the upper surface under the three lighting schemes, the flange is flipped by the air pump flipping system. The flipped flange is sent back to the lighting system to inspect its lower surface. Finally, the flange will be unloaded at different positions depending on the inspection result.

### 2.1. Visual-detection-simulating sensing method with an active lighting system

Optical inspection based on machine vision is used in this study for the surface defect detection of flanges. Owing to the characteristics of metal workpieces, a suitable lighting system that can minimize the interference of reflection and noise is required. In manual inspection, workers always rotate the flange to find proper observation angles, which determine the position of a reflection. By imitating their detection method, a multi-angle lighting system is designed. According to investigations and experiments, we found that the combination of brightfield and darkfield illumination can highlight different types of defects. To obtain suitable images for

subsequent processing, we designed a bionic active lighting and imaging system that mimics workers who detect defects under horizontal light. It is a combination of multi-angle illumination, darkfield illumination, and brightfield illumination.

As shown in Figure 4, the lighting system consists of two cameras, an annular light, and side light sources, of which the outer frame is covered by light-absorbing materials to form a dark room. The annular light illuminates vertically, from top to bottom, while the side-lights illuminate horizontally inwards. Side-light sources are made of rectangular strips that can be controlled individually. Each strip is equipped with three rows of LEDs and is covered with light-softening plates. The top and side-lights adopt the principles of brightfield illumination and darkfield illumination, respectively. Considering the monochromatic flange surface, only white LEDs were used. To capture the various profiles of the flange, the imaging system uses a camera arrangement with a 45° angle side camera and a top camera. Thus, the details of the flange surface can be clearly captured.

The design of the side light source adopts a multi-angle illumination principle. For metal surfaces, defect image perceptions are greatly affected by the lighting angle (Zhou, Liang, and Wei 2016). A previous study (Chantler 1995) proved that

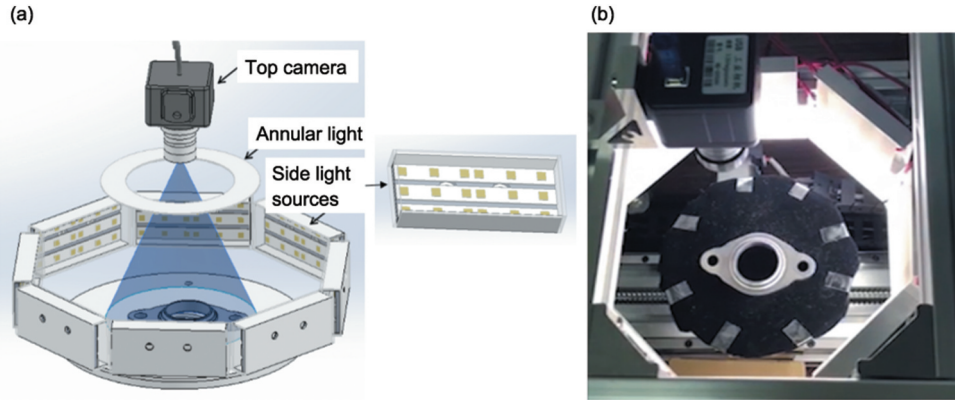


**Figure 4.** (a) Illustration of illumination design; (b) photography of the lighting system.

the surface texture of material appears differently under different light angles. Illumination perpendicular to the angle of the defect makes its image clearer. Liao et al. (2010) designed a multi-angle illumination method, which performs an important function in the inspection. The side lights can be separately controlled to achieve multi-angle illumination, and the lighting schemes are introduced in Section 4.1.

Brightfield and darkfield illumination can, respectively, highlight different types of defects. Under brightfield illumination,

light enters the camera through reflection, while under dark-field illumination it does not. The surface of the flange illuminated by the side light does not present a bright image, but defects with a 3D structure turn brighter. A previous study used dark-field imaging systems to detect surface defects of optical elements and confirmed that the system easily observes small flaws (Tao et al. 2015). As shown in Figure 5, the experiments indicate that darkfield illumination provides a uniform light effect on surfaces. Defects such as scratches appear as light-

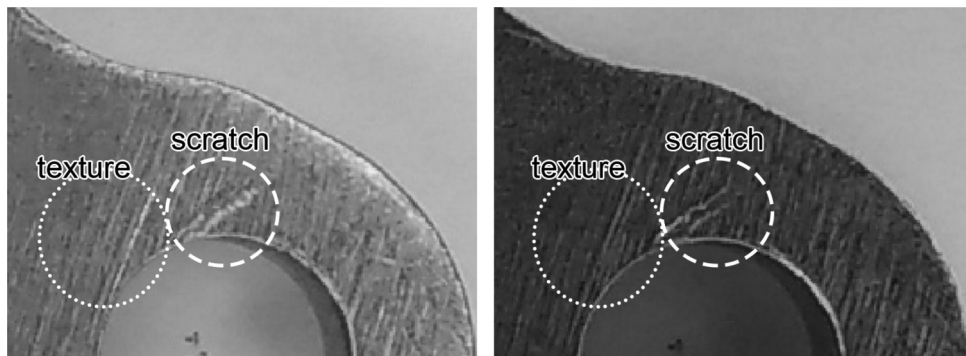


**Figure 5.** Scratch images under brightfield (left) and darkfield (right) illumination.

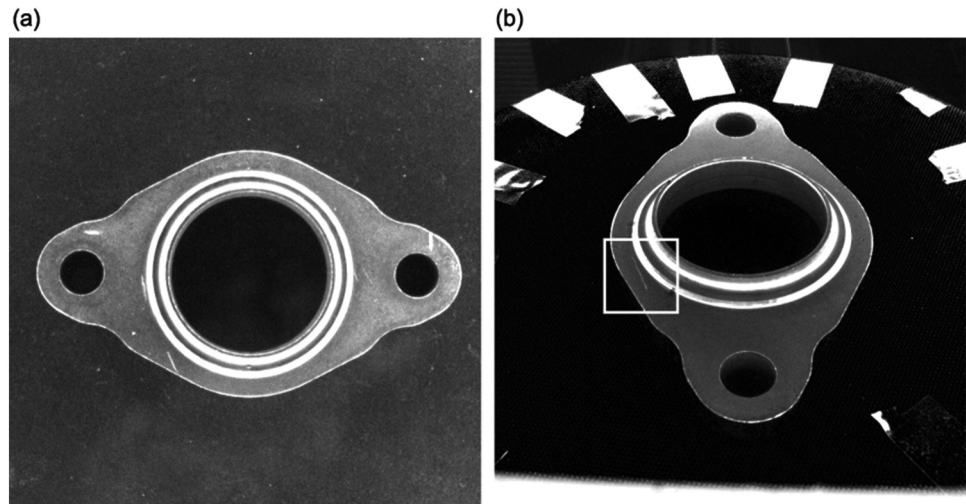


**Figure 6.** Images from two shooting angles: (a) image from the top camera, and (b) image from the side camera.

colored areas and the surface texture is faded. Brightfield illumination is better for sunken defects, such as imprints.

The lighting system we designed can eliminate interference caused by reflections. The specific methods can be summarized as follows: a) Focus on the reflection at edges and defects b) Blur the boundaries between reflections and dark surfaces. In Figure 6(a), when the side lights are all turned on, the edges of the flange can be clearly seen in the top camera, and defects can be easily distinguished. Figure 6(b) is taken by the side camera when only the opposite lights are turned on. There are no obvious reflective spots in the image. The evaluation of multi-angle illumination will be further discussed in Section 4.1.

## 2.2. Human-operation simulating method with multi-angle imaging platform

During manual inspection, workers adjust the viewing position by rotating and flipping the flange. To mimic this mode of operation, a mechanical structure is designed. Movements and illumination can be dynamically matched to simulate manual inspection.

The multi-angle imaging platform consists of a rotating platform, a slideway, and an air-pump flipping system. By changing the shooting angle, the rotating platform adjusts the angle of illumination on the flange surfaces and captures the sides of the flange using the side camera. The air pump flipping system is designed to turn over the surface for image acquisition on the back. The slideway serves as a flange transporter to carry objects from one work position to the others.

The rotating platform needs to rotate 360° for each inspection. High precision and repetitive positioning accuracy are

required to ensure the stable operation of the system. The encoder is equipped to minimize the occurrence of lost steps. Finally, a worm-gear rotating platform is chosen.

The three-DOF (Degree of Freedom) air pump flipping system can steadily flip the flange. The pneumatic finger was fixed to the front end with a silicone-wrapped gripper to grasp the flange.

## 2.3. Recognition algorithm based on the human visual decision mechanism

This study designed an image segmentation and defect recognition algorithm based on the human-visual decision mechanism. It imitates the way human attention is focused. Guo, Zhao, and Jiang (2017) designed a defect-recognition algorithm for steel plates based on the human visual attention mechanism. By observing the characteristics of the manual visual inspection, we found that workers often search for suspected sites from one surface to the other, and then further observe the site to determine whether it is really a defect. Imitating the behavior of workers, we designed such detection methods: First, the position of the flange in the picture is determined by fixing the shooting position and angle. Second, according to the edges, areas corresponding to different surfaces of the flange are divided. Finally, defects are found by the recognition algorithm. The algorithm functions are implemented using Halcon software.

In the pre-processing, different color channels under different background cloths were compared. Figure 7 shows that black cloths make the edge between the flange and background unclear. By changing to red cloths, the colors of the

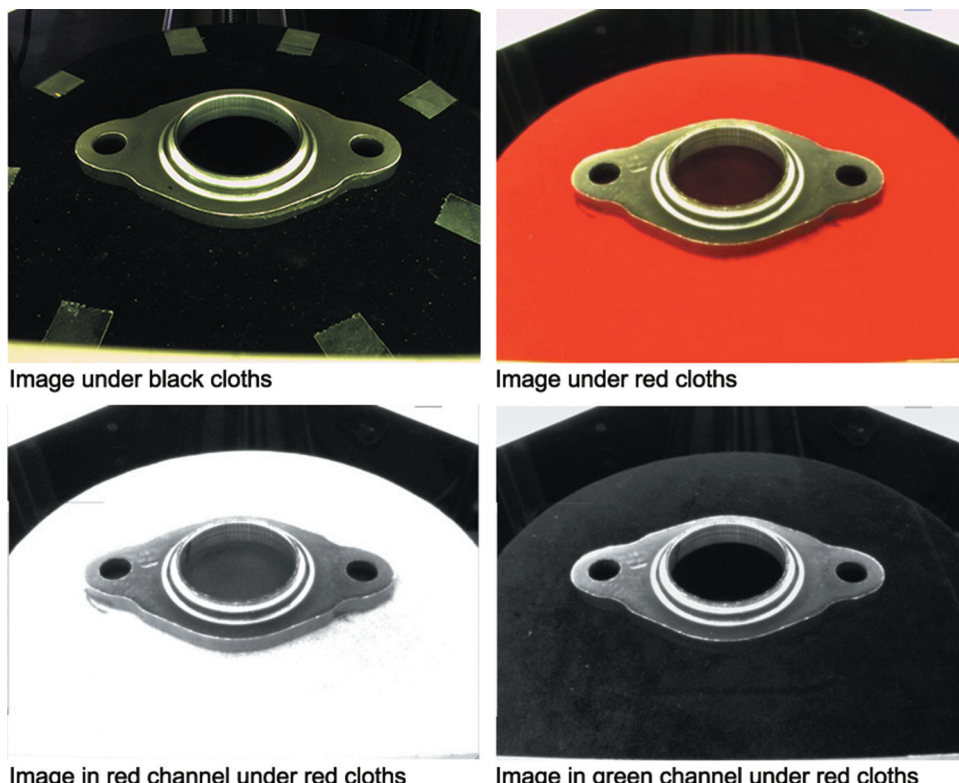


Figure 7. Original images and grayscale images under different background.

flange and the background can be clearly distinguished. The grayscale image in the red or green channel is also displayed in Figure 7. The image in the green channel under red cloths is best for extracting the contour of the upper surface.

High-resolution images require filtering, otherwise, it will be impossible to obtain continuous edges. Zhang et al. (2018) applied filters to eliminate the influence of noise from reflection and surface texture. Figure 8 presents the original image and the filtered images. The low-pass filter effectively removes redundant edge information and obtains smoother edges.

To implement the low-pass filtering process, the picture needs to be transferred to the frequency domain through the discrete Fourier transform, then convolved with the low-pass filter, and finally transferred to the spatial domain by the inverse discrete Fourier transform. Taking the function  $f(x, y)$  whose image size is  $M \times N$  as an example, the discrete Fourier transform and inverse transform formula are as follows:

$$F(u, v) = \sum_{x=0}^{M-1} \sum_{y=0}^{N-1} f(x, y) e^{-j2\pi(\frac{ux}{M} + \frac{vy}{N})}, \quad (1)$$

$$f(x, y) = \frac{1}{MN} \sum_{u=0}^{M-1} \sum_{v=0}^{N-1} F(u, v) e^{j2\pi(\frac{ux}{M} + \frac{vy}{N})}, \quad (2)$$

In this case, the Butterworth filter is used. Its formula is as follows:

$$H(u, v) = \frac{1}{1 + \left(\frac{D(u, v)}{D_0}\right)^{2n}}, \quad (3)$$

To extract edges well, we investigated various edge extraction operators. Previous work (Öztürk and Akdemir 2015) conducted a detailed comparison of several common edge extraction operators in the inspection of glass products, and concluded that under high noise, the Canny operator and LoG (Laplacian of Gaussian) operator are superior to other operators in terms of accuracy. We also compared the results of Sobel, Laplacian, and Canny operators for the edge extraction of flanges, among which the Canny operator performs the best with the fewest extra lines. Hence, the Canny operator is chosen. The specific calculation process is as follows. First, the image to be tested is smoothed by a Gaussian filter. Second, the first-order partial derivative of the row-column filter smoothed by Gaussian filtering is approximated, and the amplitude and direction of the gradient ( $\mathbf{G}_x, \mathbf{G}_y$ ) are obtained by the following formula:

$$\Psi_x = \frac{1}{2} \cdot \begin{bmatrix} -1 & 1 \\ -1 & 1 \end{bmatrix}, \quad \Psi_y = \frac{1}{2} \cdot \begin{bmatrix} 1 & 1 \\ -1 & -1 \end{bmatrix} \quad (4)$$

$$\mathbf{G}_x = \Psi_x * f(x, y), \quad \mathbf{G}_y = \Psi_y * f(x, y) \quad (5)$$

$$G = \sqrt{\mathbf{G}_x^2 + \mathbf{G}_y^2}, \quad \theta = \arctan\left(\frac{G_y}{G_x}\right) \quad (6)$$

The third step is a non-maximum suppression, to sharpen the blurred edges. Finally, to optimize the poor continuity of the Canny edge detector, the result is connected.

After the edge extraction, the correct edge of the upper surface is to be picked from the results. To this end, several regions of interest (ROIs) generated by the edges are sorted in

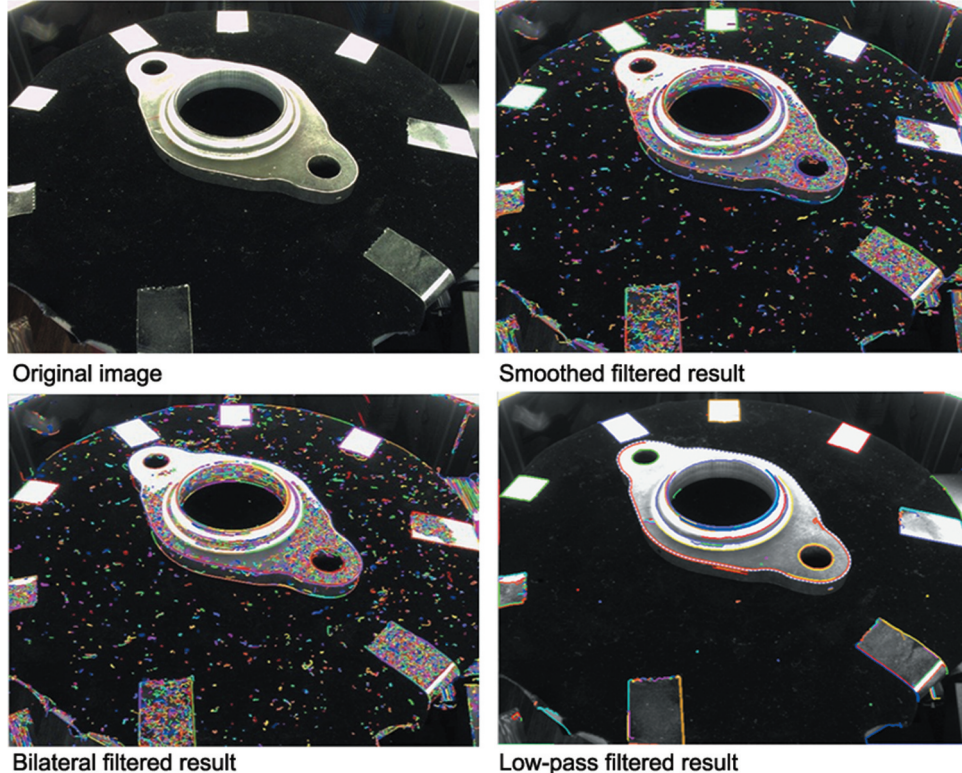
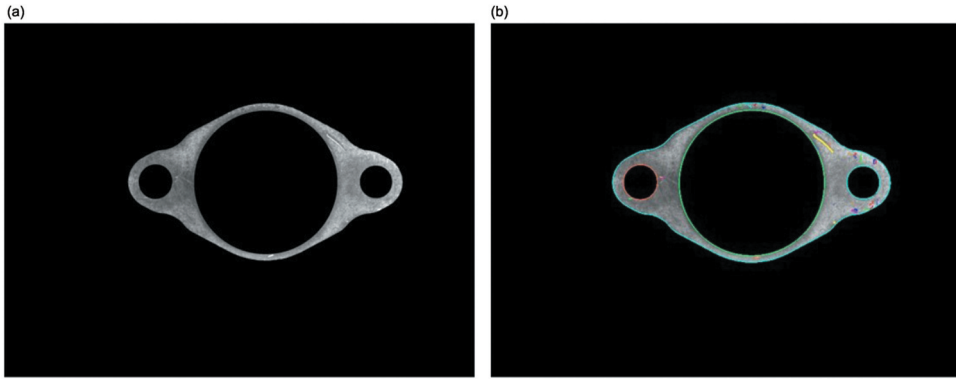


Figure 8. Extraction results.



**Figure 9.** Upper surface segmentation and defect-recognition: (a) upper surface segmentation, and (b) contour of the upper surface and defects.

descending order according to the area size. The position of the flange in the image and the pixels occupied by its surface are calculated from the real dimensions in the drawing and its distance from the cameras. After corrosion and expansion, the area ranges of the upper surface area, the center hole, and bolt holes were determined. The edge whose ROI area falls in the calculated area range is the solution. The segmentation of the upper surface is shown in Figure 9(a).

Through the same procedure, the complete upper surface contour and the upper surface defect contour can be obtained. The results are shown in Figure 9(b).

Taking the detected defect position as the center, crop the  $256 \times 256$ -pixel defect samples as shown in Figure 10.

Because image processing is sensitive to parameters, important parameters in the algorithm are designed to be adaptive. They are: the frequency of the low-pass filter, high threshold of the Canny operator, the low threshold of the Canny operator, and edge connection neighborhood. After adaptation, the frequency of the low-pass filter has four different values, most of which are 0.2, and a few are 0.15, 0.1, 0.4. The high and low thresholds of the Canny operator are set to 40 and 10 respectively, while edge connection neighborhood is set as 5.

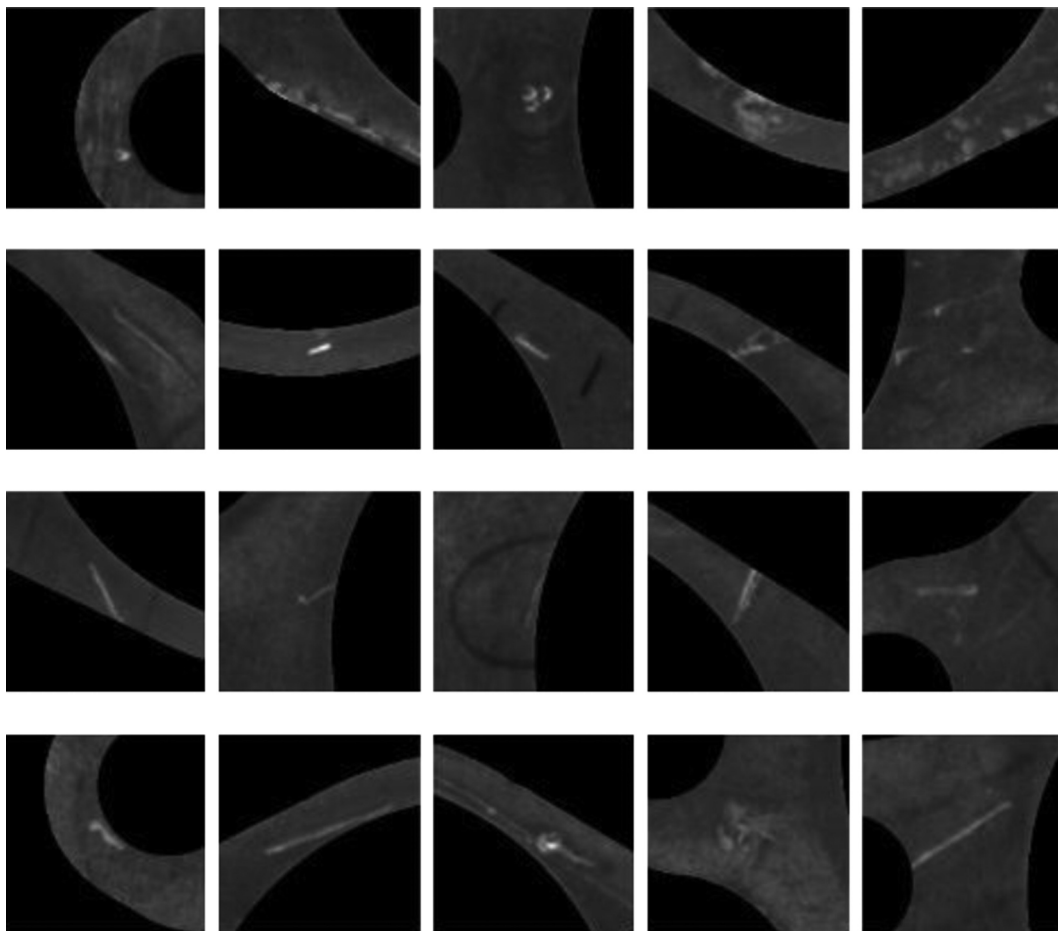


**Figure 10.** Defect samples.

The core algorithm is edge extraction by the Canny operator, which is also the most complex part. The computational complexity is  $O(M \cdot N \cdot \log(M \cdot N))$ , and the space complexity is  $O(M \cdot N)$ . The hardware is an i7 processor with 2GB of memory, no GPU. It stands to reason that the real-time performance will be enhanced if GPUs are available.

### 3. Experimental setup

The experimental setup is displayed in Figure 11. In addition to the active lighting system and bionic-operation mechanical structure mentioned in previous chapters, the entire automatic detection platform also includes a touch screen and an IPC (Industrial PC). In this chapter, we will introduce the electro-mechanical structure and hardware test results.

#### 3.1. Electromechanical structure

The mechanical structure needs to integrate the following modules: (1) A lighting system: Consisting of 8 rectangular LED strips at the sides and an annular light on the top, controlled separately. Two 5-megapixel industrial cameras are mounted on the top and side of the lighting platform. (2) Slideway: Connected to the rotating platform for transporting the flange. The lead is 0.8 m and the maximum velocity is 0.1 m/s. (3) Rotating platform: connected to the slide table, a round table of diameter 160 mm is mounted to place the flange. The load is 30 kg. The resolution is 0.001° under 20 subdivisions, and the maximum velocity is 50°/s. (4) The air pump flipping system is used to flip the flange. The gripper captures the flange and can tolerate positional deviation. (5) An integrated circuit board ensures the correct operation of the mechanical structure.

The touch-enabled screen is equipped to facilitate user operation. Three main interfaces are the process display interface, manual control interface, and statistical interface. IPC is used to control two cameras, to process and store the images.

#### 3.2. Hardware testing results

During testing, the electromechanical system runs steadily and continuously for 32,760 s (546 min) without fault. In 182 transmission measurement cycles, the rotating platform has no step loss, and the images obtained by the top camera of 800 rotating cycles are completely coincident, which also means that the hardware has very little positioning error.

### 4. Evaluation and discussion

In this study, 100 randomly chosen defective flanges were tested. The test consists of imaging effects under different lighting schemes, profile segmentation, and defect detection success rates. The feasibility and performance of the method are evaluated.

#### 4.1. Lighting and imaging evaluation

To fully obtain the defect image, three different schemes are selected under theoretical demonstration and experiments (Figure 12). In scheme 1, all eight light bands on the platform are illuminated so that the flange can be imaged under uniform illumination. In scheme 2, five lights close to the side camera are turned on to illuminate the flange in the uniform front light. In the last one, three lights opposite to the camera are turned on to show the flange in uniform backlighting.

Under scheme 1, the algorithm performs well in splitting all surfaces that need to be tested (Figure 13), which is summarized as follows: (a) upper surface, (b) bolt holes on the upper surface, (c) the lower surface, (d) the center hole on the lower surface, and (e) side.

Figure 14 shows the images of the lower surface under the three schemes. Uniform illumination under scheme 1 lights up the entire donut area while the other two only light up a half. Imprint circled in the figure is clearly captured under scheme 3.

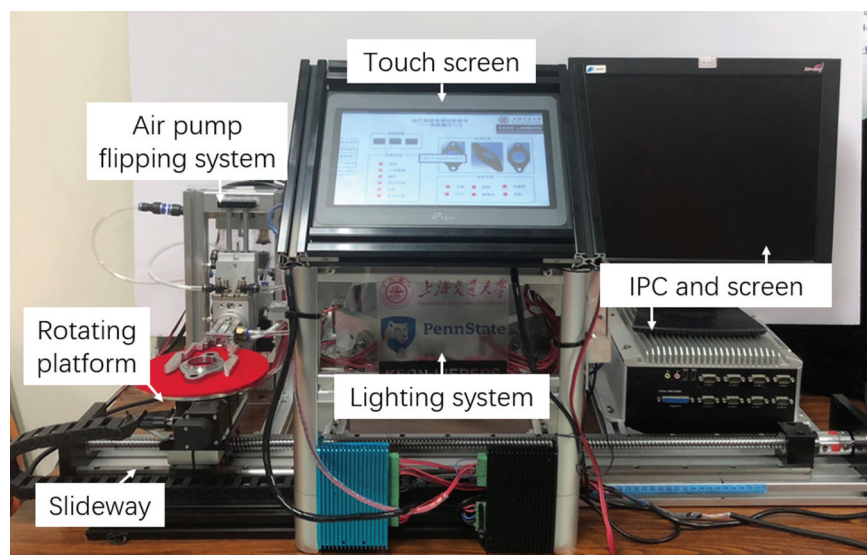
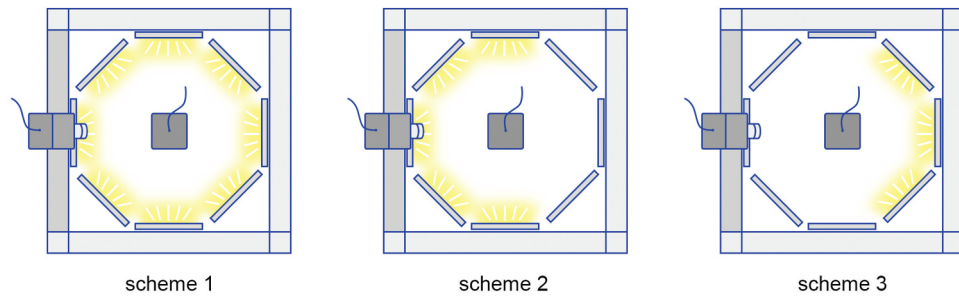
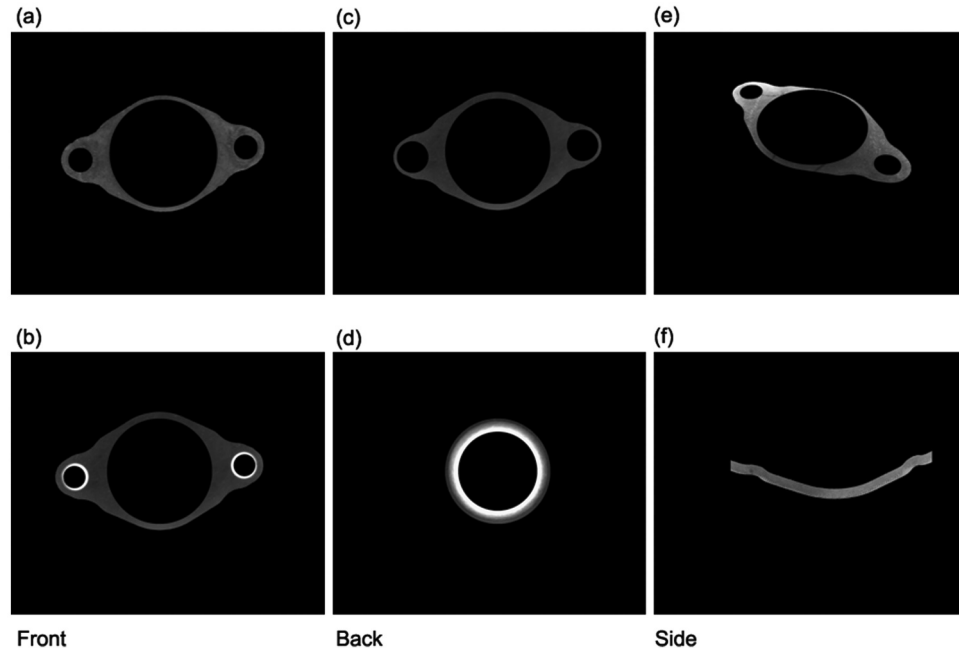


Figure 11. Photography of the experimental setup.



**Figure 12.** Illustration of three lighting schemes.



**Figure 13.** Segmentation result of two cameras.

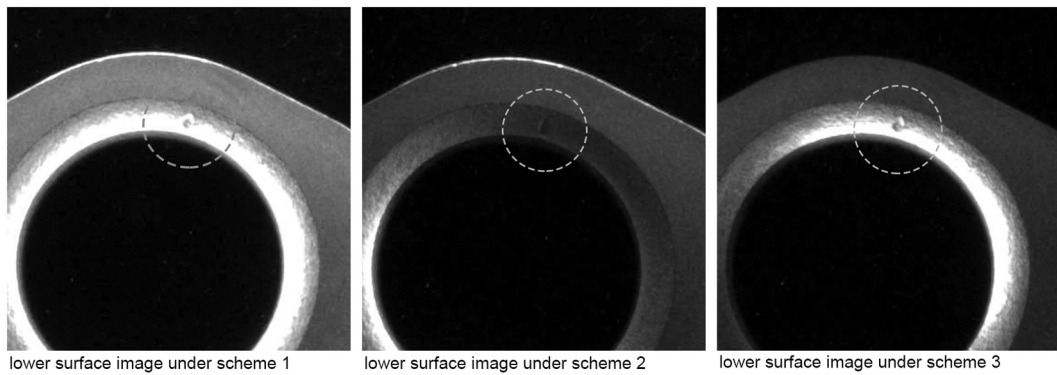


**Figure 14.** Comparison among three schemes.

Schemes 2 and 3 are also effective for the side camera. As shown in Figure 15, the slight scratch circled becomes a uniform bright area only when it is illuminated under scheme 2.

#### 4.2. Segmentation and recognition

Multi-angle profile segmentation and defect detection tests were carried out for the 100 defective flange samples.

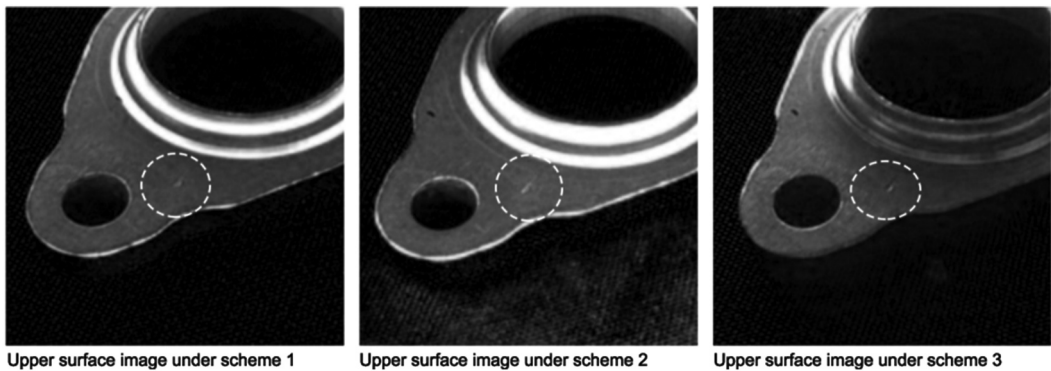


**Figure 15.** Images from side camera under three schemes.

**Table 1.** Result of the top camera.

Function	Segmentation rate (%)	Miss detection number	Miss detection rate (%)
Segmentation/detection of upper surface	97.00	5	5.20
Segmentation/detection of lower surface	98.00	0	0.00
Segmentation/detection of center hole	98.00	2	2.00
Detection of small holes' chamfer	85.00	(not provided)	(not provided)

**Table 2.** Result of the side camera in scheme 1.

Angle (°)	Segmentation surface	Segmentation rate (%)
0	Upper surface	86.00
	Lower surface	85.00
	Side	87.00
45	Upper surface	86.00
	Lower surface	85.00
	Side surface	89.00
90	Upper surface	85.00
	Lower surface	84.00
	Side	86.00
135	Upper surface	86.00
	Lower surface	85.00
	Side	89.00

**Table 3.** Result of the side camera in scheme 2 and 3.

Angle (°)	Lighting scheme	Segmentation surface	Segmentation rate (%)
0	2	Upper surface	86.00
		Lower surface	85.00
	3	Upper surface	86.00
		Lower surface	85.00
45	2	Upper surface	86.00
		Lower surface	85.00
	3	Upper surface	86.00
		Lower surface	85.00
90	2	Upper surface	85.00
		Lower surface	85.00
	3	Upper surface	85.00
		Lower surface	84.00
135	2	Upper surface	86.00
		Lower surface	84.00
	3	Upper surface	86.00
		Lower surface	85.00

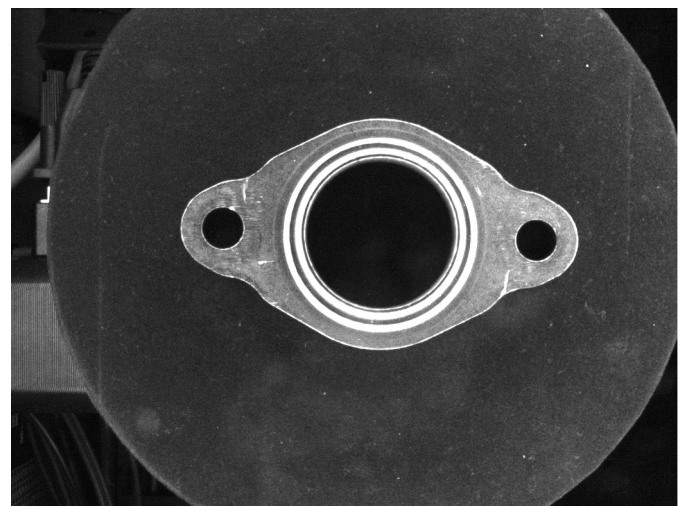


**Figure 16.** Missed detection of the circular scratch.

Because most sample defects are on the upper surface, test results of the upper surface are shown. **Tables 1–3** present the results of the segmentation rate and miss detection rate. The segmentation rate is the ratio of the successfully segmented number to the test number; the miss detection rate is the ratio of the missed detection number to the successfully segmented number.

From the tables, the top camera has a profile segmentation rate over 95%, while the side camera has a segmentation rate of approximately 85%. The missed detections on the upper surface are several shallow pit defects and a regular-shaped circular scratch, whereas shallow pit defects are all recognized in the image of the side camera. However, the missing circular scratch presents as a circle around the center hole (**Figure 16**), which is too large to be recognized. To solve this problem, it is necessary to incorporate other detection methods.

#### 4.3. Feasibility and performance

The ability of the system to obtain omnidirectional multi-view images of the flange and detect different kinds of defects distributed on the respective surfaces is evaluated.

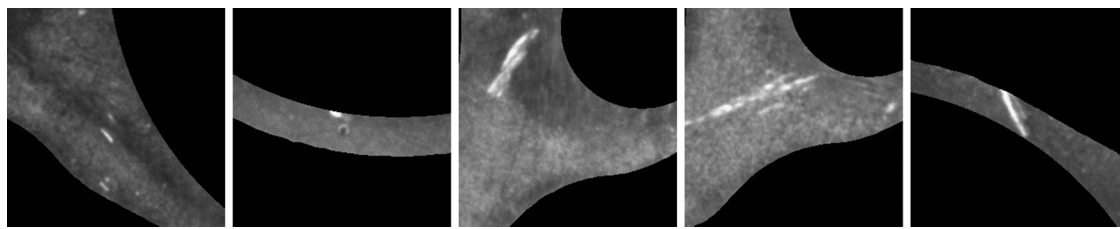


**Figure 17.** Defect samples of different scales and locations.

To analyze the complex structure of the flange, the detecting system obtains the images from multiple angles, and the required profiles using the segmentation algorithm. From the test results in Section 4.2, it is evident that the top camera can capture the most defects, while the missing defects can be identified in the side camera under lighting schemes 2 and 3, except for one case. Thus, the multi-angle and multi-lighting scheme detecting method is superior for detecting surface defects of complex structures.

The defect samples in Figure 17 indicate the different scales and locations of the defects detected. Through calculation, the maximum resolution captured image can display defects as small as 0.05 mm, while the smallest defect in the samples is 0.1 mm. Although human eyes can recognize defects at this scale, repetitive tiring work reduces concentration, and may even lead to omitted inspections. For a visual check at a high detecting pace of 30 s per workpiece, only defects greater than 0.3 mm can be identified reliably.

Compared to conventional methods, the automated method we have provided here is more time-consuming. Manual detection takes 30 s every time, while the automated method takes 80–90 s. Since the images are synchronously processed, the movement of hardware consumes the most time. The factors that affect the detection speed are listed: (a) Mechanical structure: velocities of the rotating platform and slideway are limited to 33°/s and 0.1 m/s. It also takes 3.7 s to flip a flange. (b) The response of the cameras is slightly delayed, and when the light scheme is changed, they need approximately 2 s to adapt.

The detection efficiency can be improved with upgraded hardware. Moreover, if an additional work position is added, the upper and lower surfaces can be separately inspected, and thus the average detection time can be shortened. Although the proposed automated method requires further improvements, it can continuously function for a long time and seamlessly link with robotic logistics, which is preferable to manual inspection.

Compared to the existing AOI method, the proposed inspection method has a wider range of applications. The system built in this study can detect objects with three-dimensional structures and can detect multiple surfaces, which is not possible using other methods for steel plates, tiles and glass mentioned in the references. In addition, the interferences can be suppressed by the active lighting system. It is also able to detect insignificant and subtle defects.

In summary, the algorithm achieves a 1% miss detection rate on the upper surface, and realizes flange's profile segmentation, defect detection and defect marking under different illumination conditions and angles.

## 5. Conclusion

To solve the generic problem of surface defect inspection on reflective metal workpieces, an automatic apparatus with a generic mechatronics design methodology widely applicable to metal workpiece surface quality inspection in the manufacturing industry is designed. Using light source selection, viewing angle switching and attention mechanism, human worker behavior is mimicked to realize an automatic detection system for complex surfaces. The method can cover the full view of flanges, and obtain complete side information.

This study proposes an automatic optical inspection with bionic motion-vision paradigm for surface quality inspection of workpieces with complex structures and subtle defects. Defects of highly reflective metal workpieces are detected under the active lighting system, which weakens the influence of reflection and noise. The surface segmentation and defect detection algorithms designed in this study identify defects with a minimum width of 0.1 mm, with a detection rate of more than 95%, which meets the expected intelligent detection requirements. This research provides a universally applicable method for surface defect detection of complex surfaces.

## Nomenclature

$D_0$  the cutoff frequency of the Butterworth filter

$D(u, v)$  distance from  $(u, v)$  to the origin

$F(u, v)$  matrix of an image in frequency domain

$f(x, y)$  matrix of an image in spatial domain

$G$  amplitude and direction of the gradient

$G_x, G_y$  gradients in x and y directions

$H(u, v)$  result of lowpass filter

$h(x, y)$  result of Gaussian function

$M, N$  dimensions of image matrix

n	order of the Butterworth filter
$u, v$	variables in frequency domain
$x, y$	variables in spatial domain
$\theta$	direction of the gradient
$\sigma$	standard deviation in Gaussian function
$\Psi_x, \Psi_y$	operators used to calculate first-order gradients of images

## Acknowledgments

The authors gratefully thank A/Prof. Timothy Wheeler from Penn State University, Mrs. Lu Chen and Mrs. Yanping Lin from Shanghai Jiao Tong University for their valuable suggestions.

## Disclosure statement

No potential conflict of interest was reported by the authors.

## Funding

The work has been supported by National Natural Science Foundation of China under Grant No. 51775333, as well as Natural Science Foundation of Jiangsu Province under Grant No. BK20171250.

## References

- Abbas, M., and M. Shafiee. 2018. "Structural Health Monitoring (SHM) and Determination of Surface Defects in Large Metallic Structures Using Ultrasonic Guided Waves." *Sensors* 18 (11): 3958. doi:[10.3390/s18113958](https://doi.org/10.3390/s18113958).
- Chantler, M. J. 1995. "Why Illuminant Direction Is Fundamental to Texture Analysis." *IEE Proceedings-Vision, Image and Signal Processing* 142 (4): 199–206. doi:[10.1049/ip-vis:19952065](https://doi.org/10.1049/ip-vis:19952065).
- Chiou, Y.-C., and W.-C. Li. 2009. "Flaw Detection of Cylindrical Surfaces in PU-packing by Using Machine Vision Technique." *Measurement* 42 (7): 989–1000. doi:[10.1016/j.measurement.2009.02.006](https://doi.org/10.1016/j.measurement.2009.02.006).
- Da, Y., G. Dong, B. Wang, D. Liu, and Z. Qian. 2018. "A Novel Approach to Surface Defect Detection." *International Journal of Engineering Science* 133: 181–195. doi:[10.1016/j.ijengsci.2018.09.005](https://doi.org/10.1016/j.ijengsci.2018.09.005).
- Grijalba, F. A. F., and L. R. Padovese. 2018. "Non-Destructive Flaw Mapping of Steel Surfaces by the Continuous Magnetic Barkhausen Noise Method: Detection of Plastic Deformation." *Journal of Nondestructive Evaluation* 37 (2): 26. doi:[10.1007/s10921-018-0480-6](https://doi.org/10.1007/s10921-018-0480-6).
- Guo, F., J. Zhao, and P. Jiang. 2017. "Surface Defects Detection of Steel Plate Based on Visual Attention Mechanism." In *2017 Chinese Automation Congress(CAC)*, 3174–3177. Jinan, China, October 20–22. NewYork: IEEE.
- Guo, Z., D. Zhang, Y. Tan, F. Shi, B. Zhang, and J. Gong. 2015. "Ultrasonic Phased Array on the Inner Surface of Circular Stage for Detecting the Circumferential Flaw in a Pipe." In *2015 IEEE International Ultrasonics Symposium*, 1–4. Taipei, Taiwan, October 21–24. NewYork: IEEE.
- Gusev, A. P. 2015. "Hysteresis of the Magnetic Field of Surface Flaws in Different Steels during Magnetization with an Attachable Electromagnet." *Russian Journal of Nondestructive Testing* 51 (10): 616–623. doi:[10.1134/s1061830915100058](https://doi.org/10.1134/s1061830915100058).
- Hanzeai, S. H., A. Afshar, and F. Barazandeh. 2017. "Automatic Detection and Classification of the Ceramic Tiles' Surface Defects." *Pattern Recognition* 66: 174–189. doi:[10.1016/j.patcog.2016.11.021](https://doi.org/10.1016/j.patcog.2016.11.021).
- Huang, M.-S., and H.-Y. Chiu. 2009. "Surface Defect Inspection of Light Guided Plates with the Computer-vision Assisted Detection Method." *Journal of the Chinese Institute of Engineers* 32 (2): 179–191. doi:[10.1080/02533839.2009.9671496](https://doi.org/10.1080/02533839.2009.9671496).
- Jovančević, I., -H.-H. Pham, -J.-J. Orteu, R. Gilblas, J. Harvent, X. Maurice, and L. Brèthes. 2017. "3D Point Cloud Analysis for Detection and Characterization of Defects on Airplane Exterior Surface." *Journal of Nondestructive Evaluation* 36 (4): 74. doi:[10.1007/s10921-017-0453-1](https://doi.org/10.1007/s10921-017-0453-1).
- Kasai, N., and K. Miura. 2012. "Detection of a Surface Flaw Using Differential Signals of MI Sensors with the Residual Magnetization Method." In *ASME 2012 Pressure Vessels and Piping Conference*, 241–244. Toronto, Ontario, July 15–19. New York: ASME.
- Kong, Q., Z. Yu, Y. Zhao, H. Wang, and Z. Lin. 2017. "A Study of Severe Flange Wrinkling in First-Pass Conventional Spinning of Hemispherical Part." *International Journal of Advanced Manufacturing Technology* 93 (9–12): 3583–3598. doi:[10.1007/s00170-017-0744-9](https://doi.org/10.1007/s00170-017-0744-9).
- Liao, Y., X. Weng, C. W. Swonger, and J. Ni. 2010. "Defect Detection and Classification of Machined Surfaces under Multiple Illuminant Directions." In *Proceedings of SPIE Optical Engineering + Applications*, 77981T. San Diego, California, United States, August 2–4. Washington, DC: SPIE.
- Lu, J., H. Zhao, and Y. Qu. 2006. "Research on Automatic Detection Method of Non-uniform Reflective Metal Sphere's Surface Flaws." In *Proceedings of Sixth International Symposium on Instrumentation and Control Technology*, 63570P. Beijing, China, October 13–15. Washington, DC: SPIE.
- Öztürk, S., and B. Akdemir. 2015. "Comparison of Edge Detection Algorithms for Texture Analysis on Glass Production." *Procedia - Social and Behavioral Sciences* 195: 2675–2682. doi:[10.1016/j.sbspro.2015.06.477](https://doi.org/10.1016/j.sbspro.2015.06.477).
- Öztürk, S., and B. Akdemir. 2018. "Fuzzy Logic-based Segmentation of Manufacturing Defects on Reflective Surfaces." *Neural Computing & Applications* 29 (8): 107–116. doi:[10.1007/s00521-017-2862-6](https://doi.org/10.1007/s00521-017-2862-6).
- Sugimoto, T., and T. Kawaguchi. 1998. "Development of a Surface Defect Inspection System Using Radiant Light from Steel Products in a Hot Rolling Line." *IEEE Transactions on Instrumentation and Measurement* 47 (2): 409–416. doi:[10.1109/19.744183](https://doi.org/10.1109/19.744183).
- Tao, X., Z. Zhang, F. Zhang, and D. Xu. 2015. "A Novel and Effective Surface Flaw Inspection Instrument for Large-Aperture Optical Elements." *IEEE Transactions on Instrumentation and Measurement* 64 (9): 2530–2540. doi:[10.1109/tim.2015.2415092](https://doi.org/10.1109/tim.2015.2415092).
- Wang, Y., D. Wen, and Z. Song. 2017. "Design of Inspection System for Surface Defects on Industrial Parts under Complex Background." In *Proceedings of Applied Optics and Photonics China*, UNSP 104620P. Beijing, China, June 4–6. Washington, DC: SPIE.
- Xu, L. M., Z. Q. Yang, Z. H. Jiang, and Y. Chen. 2017. "Light Source Optimization for Automatic Visual Inspection of Piston Surface Defects." *International Journal of Advanced Manufacturing Technology* 91 (5–8): 2245–2256. doi:[10.1007/s00170-016-9937-x](https://doi.org/10.1007/s00170-016-9937-x).
- Xu, Y., F. Gao, and X. Jiang. 2018. "Enhancement of Measurement Accuracy of Optical Stereo Deflectometry Based on Imaging Model Analysis." *Optics and Lasers in Engineering* 111: 1–7. doi:[10.1016/j.optlaseng.2018.07.007](https://doi.org/10.1016/j.optlaseng.2018.07.007).
- Ye, R., C.-S. Pan, M. Chang, and C.-P. Hsieh. 2018. "In-line Inspection of Surface Feature and Defect." *Microsystem Technologies* 24 (8): 3233–3240. doi:[10.1007/s00542-017-3678-0](https://doi.org/10.1007/s00542-017-3678-0).
- Zhang, H., X. Jin, Q. M. J. Wu, Y. Wang, Z. He, and Y. Yang. 2018. "Automatic Visual Detection System of Railway Surface Defects with Curvature Filter and Improved Gaussian Mixture Model." *IEEE Transactions on Instrumentation and Measurement* 67 (7): 1593–1608. doi:[10.1109/tim.2018.2803830](https://doi.org/10.1109/tim.2018.2803830).
- Zhou, Q., R. Chen, B. Huang, C. Liu, J. Yu, and X. Yu. 2019. "An Automatic Surface Defect Inspection System for Automobiles Using Machine Vision Methods." *Sensors* 19 (3): 644–661. doi:[10.3390/s19030644](https://doi.org/10.3390/s19030644).
- Zhou, S., D. Liang, Y. Wei. 2016. "Automatic Detection of Metal Surface Defects Using Multi-Angle Lighting Multivariate Image Analysis." *2016 IEEE International Conference on Information and Automation*, Ningbo, China, August 1–3. NewYork: IEEE.